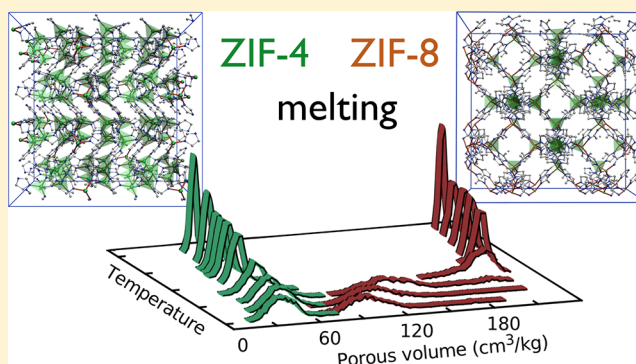


# Melting of Zeolitic Imidazolate Frameworks with Different Topologies: Insight from First-Principles Molecular Dynamics

Romain Gaillac,<sup>†,‡</sup> Pluton Pullumbi,<sup>‡</sup> and François-Xavier Coudert<sup>\*,†</sup><sup>†</sup>Institut de Recherche de Chimie Paris, Chimie ParisTech, PSL Research University, CNRS, 75005 Paris, France<sup>‡</sup>Centre de Recherche Paris Saclay, Air Liquide, 78354 Jouy-en-Josas, France**S** Supporting Information

**ABSTRACT:** Metal–organic frameworks are chemically versatile materials and are excellent candidates for many applications from carbon capture to drug delivery, through hydrogen storage. While most studies so far focus on the crystalline MOFs, there has been a recent shift to the study of their disordered states, such as defective structures, glasses, gels, and very recently liquid MOFs. Following the publication of the melting mechanism of zeolitic imidazolate framework ZIF-4, we use here molecular simulation in order to investigate the similarities and differences with two other zeolitic imidazolate frameworks, ZIF-8 and ZIF-zni. We perform first-principles molecular dynamics simulations to study the melting phenomena and the nature of the liquids obtained, focusing on structural characterization at the molecular scale, dynamics of the species, and thermodynamics of the solid–liquid transition. We show how the retention of chemical configuration, the changes in the coordination network, and the variation of the porous volume in the liquid phase are influenced by the parent crystalline framework.

**■ INTRODUCTION**

Metal–organic frameworks (MOFs) appeared almost 30 years ago<sup>1</sup> in the literature, and much of the research effort and publications have been focused on the study of crystalline structures.<sup>2</sup> These microporous or mesoporous crystalline architectures, in addition to being beautiful chemical objects, exhibit very large specific surface areas and pore volumes, making them good candidates for applications such as gas sorption or heterogeneous catalysis. Moreover, their crystallinity makes them relatively easy to characterize and allows the determination of their structure, typically by X-ray crystallography. Nonetheless, there has been a recent shift, with increasingly more examples of MOFs that show defects and disorder, and the realization that this is not always detrimental to their physical or chemical properties—and thus to their performance in potential applications. There are even studies that focus on “defective by design” strategies to explore further the configurational space of organometallic structures.<sup>3</sup> In particular, several amorphous MOFs have been studied in the past few years and proposed as candidates for applications such as controlled release, irreversible trapping of harmful substances, or creating new optically active glass-like materials.<sup>4</sup> There are several ways to obtain amorphous MOFs, ranging from direct synthesis<sup>5</sup> to the amorphization of crystalline MOFs by melting and quenching,<sup>6</sup> application of mechanical pressure,<sup>7</sup> or ball-milling.<sup>8</sup>

It has been known for 15 years that inorganic zeolites can undergo temperature-induced amorphization.<sup>9–11</sup> Zeolitic

imidazolate frameworks (ZIFs) are a subgroup of particularly thermally and chemically stable MOFs exhibiting zeolitic topologies. They are formed by assembly of tetrahedra based on a metal ion and four imidazolate ligands (possibly substituted). In 2010 was published the first report of an amorphous zeolitic imidazolate framework formed by heating Zn-based framework ZIF-4.<sup>12</sup> Then Zn-based ZIF-1 and ZIF-3 and Co-based ZIF-4 were shown to amorphize upon temperature increase, while ZIF-8, ZIF-9, ZIF-11, ZIF-14, and ZIF-βqtz would decompose without undergoing a phase transition.<sup>13</sup> The only common point to the latter are their substituted ligands compared to the former which are composed of nonsubstituted imidazolate cycles. In ref 6, Bennett et al. detail the differences in behavior between ZIF-8 and ZIF-4 in terms of calorimetric and X-ray measurements. Other experiments have demonstrated the influence of the chemical change of the ligand and the topology on the melting temperature for ZIFs which can undergo thermal amorphization.<sup>14</sup> For instance, ZIF-4 was compared to TIF-4 and ZIF-62 which possess the same topology but have slightly larger ligands. Both, TIF-4 and ZIF-62, then have shown lower melting temperatures than ZIF-4.

Recently, we studied the melting mechanism of ZIF-4,<sup>15</sup> using a combined experimental and computational study, and

Received: January 12, 2018

Revised: March 12, 2018

Published: March 12, 2018

in particular relying on *in situ* variable temperature X-ray, *ex situ* neutron pair distribution function experiments, and first-principles molecular dynamics simulations. Here, we present a theoretical study on the melting mechanism of three different ZIF frameworks, namely ZIF-8, ZIF-4, and ZIF-zni, focusing on the influence of the topology of the crystalline MOF on the melting behavior and the structure of the liquid phase. From the three frameworks chosen, two are known to undergo thermal amorphization (ZIF-4, ZIF-zni), while the other one collapses before melting (ZIF-8). ZIF-8 is composed of  $\text{Zn}(\text{mIm})_2$  tetrahedra linked by Zn–N coordination bonds and has the same topology as the zeolite sodalite (SOD).<sup>16</sup> ZIF-4 and ZIF-zni are chemically very similar to ZIF-8, except for  $\text{Zn}(\text{Im})_2$  tetrahedra instead of  $\text{Zn}(\text{mIm})_2$ . ZIF-4 is porous and shares its topology with the mineral variscite (cag topology) while ZIF-zni has a nonporous dense zni topology.<sup>17</sup> ZIF-8, because of its SOD topology, is a very open and porous framework.

## METHODS

**First-Principles Molecular Dynamics.** The behavior of zeolitic imidazolate frameworks as a function of temperature was studied by means of density functional theory (DFT)-based molecular dynamics (MD) simulations, using the Quickstep module<sup>18</sup> of the CP2K software package.<sup>19</sup> We used the hybrid Gaussian and plane wave method GPW<sup>20</sup> as implemented in CP2K. The simulations were performed in the constant-volume ( $N, V, T$ ) ensemble with fixed size and shape of the unit cell. A time step of 0.5 fs was used in the MD runs, the temperature was controlled by velocity rescaling.<sup>21</sup>

The unusually large temperature at which the simulations were performed requires careful fine-tuning of the simulation protocol. In particular, the exchange-correlation energy was evaluated in the PBE approximation,<sup>22</sup> and the dispersion interactions were treated at the DFT-D3 level.<sup>23</sup> The Quickstep module uses a multigrid system to map the basis functions onto. We kept the default number of 4 different grids but chose a relatively high plane-wave cutoff for the electronic density to be 600 Ry, as already used in ref 24, and a relative cutoff (keyword REL\_CUTOFF in CP2K) of 40 Ry for high accuracy. Valence electrons were described by double- $\zeta$  valence polarized basis sets and norm-conserving Goedecker–Teter–Hutter<sup>25</sup> pseudopotentials all adapted for PBE (DZVP-GTH-PBE) for H, C and N or optimized for solids (DZVP-MOLOPT-SR-GTH) in the case of Zn.

The unit cell studied for ZIF-4 (space group  $Pbca$ ) is the orthorhombic primitive unit cell, which contains 272 atoms, with cell parameters  $a = 15.423 \text{ \AA}$ ,  $b = 15.404 \text{ \AA}$ ,  $c = 18.438 \text{ \AA}$ , and  $\alpha = \beta = \gamma = 90^\circ$ . The unit cell studied for ZIF-8 (space group  $I-43m$ ) is the orthorhombic primitive unit cell, which contains 276 atoms, with cell parameters  $a = b = c = 16.993 \text{ \AA}$ , and  $\alpha = \beta = \gamma = 90^\circ$ . The unit cell studied for ZIF-zni (space group  $P1$ ) is the primitive unit cell, which contains 272 atoms, with cell parameters  $a = 17.570 \text{ \AA}$ ,  $b = 17.613 \text{ \AA}$ ,  $c = 17.613 \text{ \AA}$ , and  $\alpha = 138.433^\circ$ ,  $\beta = 97.256^\circ$ ,  $\gamma = 97.257^\circ$ . Representative input files for the molecular dynamics simulations are available as Supporting Information and online in our data repository at <https://github.com/fxcoudert/citable-data>.

**Trajectory Analysis.** The Lindemann ratio  $\Delta$  is computed from the width of the first peaks in the different partial radial distribution functions as a measure of the fluctuation of atomic positions and interparticular distances:

$$\Delta = \frac{\text{fwhm}}{d_0} \quad (1)$$

where fwhm is the full width at half-maximum of the first partial radial distribution function peak (estimated by a Gaussian fit) and  $d_0$  corresponds to the mean interatomic distance (calculated as the maximum of the first peak), i.e.,  $d_0 = 5.95 \text{ \AA}$  for Zn–Zn and  $d_0 = 2.0 \text{ \AA}$  for Zn–N.

The coordination number for nitrogen atoms around the zinc cation is computed by taking a cutoff radius of 2.5  $\text{\AA}$ , a value chosen from the Zn–N partial radial distribution function at room temperature. We checked that the precise value used does not influence the outcome of the calculations, nor does the choice of a discontinuous criterion (vs the use of a damping function near the cutoff value).

In order to compute the total porous volume, we used the freely available software Zeo++.<sup>26–28</sup> It uses a geometric decomposition of space to compute the accessible and nonaccessible volume to a sphere of a given radius. We have taken a value a 1.2  $\text{\AA}$  simulating the porous volume as seen by a helium molecule, calculating the distribution of instantaneous total pore space (sum of the accessible and the nonaccessible volume) along the MD trajectories at each temperature.

## RESULTS

**Structural Changes upon Heating and Melting.** In order to understand the structural evolution and onset of disorder of each framework associated with an increase of temperature, we first look at the Zn–N radial distribution functions (RDF) for each system upon heating (Figure 1, top panel). In all cases, the overall trend observed is the same: the peaks around 2 and 4  $\text{\AA}$  widen, but remain present, while the other peaks flatten and ultimately disappear at very high temperature. Another common feature of interest is the fact that, above 800 K, the RDF does not go to zero between the

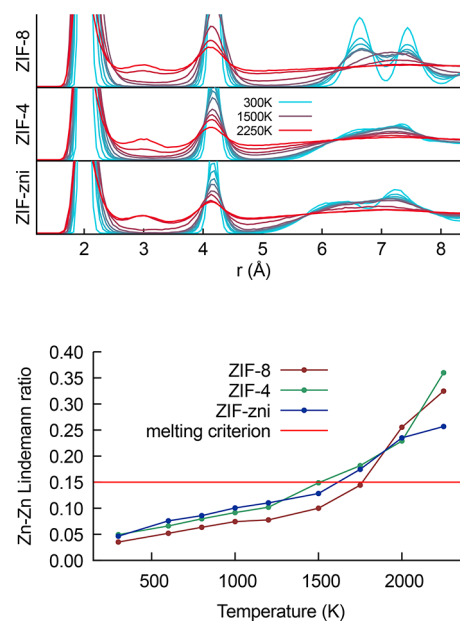


**Figure 1.** Top panel: Radial distribution functions for the pair of zinc and nitrogen atoms in the three ZIFs as a function of temperature. Bottom panel: Comparison of the evolution of the Lindemann ratios for the three ZIFs showing that melting is happening at different temperatures.

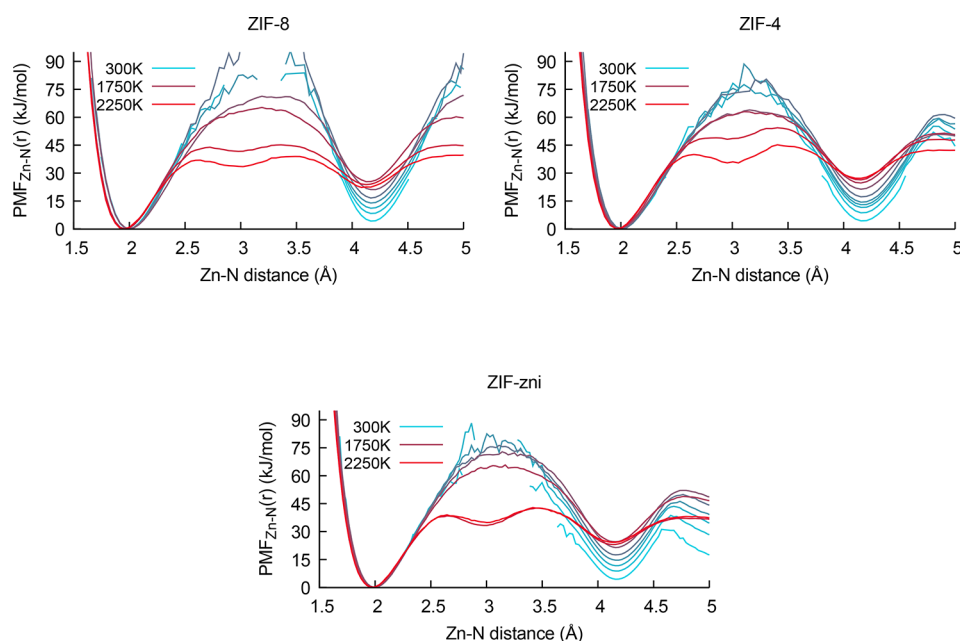


**Figure 2.** Potentials of mean force along the nitrogen–zinc reaction coordinate as functions of temperature for the three ZIFs.

first two peaks, indicating the presence of nitrogen exchanges between the first to the second coordination spheres of the zinc cations. Beyond this, we also observe differences between the different frameworks, at low and intermediate temperatures. There, ZIF-8 appears more structured than ZIF-zni, which better defined and narrower peaks; and ZIF-zni itself shows more structuration than ZIF-4. Moreover, the liquid obtained from ZIF-4 has features that are closer to its crystalline precursor than the two other frameworks. These trends observed on the partial Zn–N radial distribution functions are confirmed when we look at the total RDF (Figure S1), containing all pair of atoms, showing the crucial role of the zinc–nitrogen coordination bond in monitoring and understanding the process of melting in ZIFs.

To quantify this analysis, we computed the Lindemann ratio for the three ZIFs as a function of temperature (Figure 1 bottom panel). Computed from the width  $w$  of the first peak at distance  $d_0$  in the different partial radial distribution function, the Lindemann ratio  $\Delta = w/d_0$  is as a measure of the fluctuation of interatomic distances. A jump in the Lindemann ratio, which is rather linear at low temperature, and the crossing of the threshold value of 15%, are typically understood to evidence the melting of a solid. This occurs in the temperature range of 1200–1500 K for ZIF-4, in the range of 1500–1750 K for ZIF-zni, and above that value for ZIF-8. We can thus assign an “order” to the melting temperatures of the three frameworks, with  $T_m(\text{ZIF-4}) < T_m(\text{ZIF-zni}) < T_m(\text{ZIF-8})$ . This may explain why ZIF-8 is experimentally observed not to melt, because its melting temperature is too high compared to its decomposition temperature.

Finally, we computed the average mean square displacement per atom (summed over all atoms of a framework), over a reference length of time ( $\tau = 75$  ps). We observe on Figure S2 that diffusion really starts between 1250 and 1500 K for ZIF-4 and only above 1500 K for ZIF-8. Diffusion in ZIF-zni seems to be hindered by its very dense structure, qualitatively different from the porous structures of ZIF-4 and ZIF-8. As a result, diffusion only appears above 1750 K in this framework, whereas its Lindemann ratio at this temperature is higher than the one

for ZIF-8. The comparison between the three frameworks indicates again that ZIF-8 ordering is more affected when melting.

Although the “theoretical” melting temperatures we report are well above experimental melting temperatures (around 840 K for ZIF-4<sup>6</sup>), we believe our modeling still provides insights on the underlying mechanism happening at the “real” melting temperatures. Ab initio methods do not allow long time scales and very large systems, but by going to higher temperatures and checking the Arrhenian behavior of the rare events observed, such as bond cleavages, we are able to compare between these three frameworks.

**Thermodynamics of Melting.** In order to better understand the thermodynamics of ZIF melting, we proceeded used the Zn–N distance as a reaction coordinate, following the breaking and reformation of zinc–imidazolate coordination. From the partial radial distribution function between Zn and N,  $g_{\text{Zn-N}}(r)$ , we computed the potential of mean force (PMF),  $F(r) = -k_B T \ln g(r)$ , at all temperatures. The resulting free energy profiles are shown in Figure 2, and present similar features: the barrier at 300 K is too high to be measured (since no dissociation event is observed during the time of our simulations), and lower with increasing temperature. The barrier height, when it can be measured, is the activation free energy  $\Delta F^\ddagger$  associated with the breaking of the Zn–N coordination bond. Its temperature dependence is displayed as a van’t Hoff plot in Figure S3, and a linear approximation (van’t Hoff law,  $\Delta F^\ddagger(T) = \Delta U^\ddagger - T\Delta S^\ddagger$ ) is used in each case—with a reasonable fit—to obtain values for the activation energy and entropy,  $\Delta U^\ddagger$  and  $\Delta S^\ddagger$ , respectively. The values obtained are given in Table 1.

In all cases the free energy barrier is dominated by the energetic term, while the activation entropy brings a small stabilization at high temperature. We observe that the free energy barriers encountered at the estimated melting temperatures are of  $6k_B T$  for ZIF-8 (at 1500 K) and  $8k_B T$  for ZIF-4 and ZIF-zni (at 1200 K), significantly higher than thermal fluctuations. Thus, we confirm for ZIF-8 and ZIF-zni what was found for ZIF-4, namely that melting occurs through an

**Table 1.** Activation Enthalpy Associated with a Bond Cleavage, Activation Entropy, and Extrapolated Activation Free Energy at the Experimental Melting Temperature for ZIF-4 of 840 K

	$\Delta U^\ddagger$ (kJ mol <sup>-1</sup> )	$\Delta S^\ddagger$ (J mol <sup>-1</sup> K <sup>-1</sup> )	$\Delta F^\ddagger(840\text{ K})$ (kJ mol <sup>-1</sup> )
ZIF-8 (Zn–N)	145	48	105 ( $\approx 15kT$ )
ZIF-8 (Zn–Im)	207	77	142 ( $\approx 20kT$ )
ZIF-4 (Zn–N)	127	37	95 ( $\approx 14kT$ )
ZIF-4 (Zn–Im)	123	36	93 ( $\approx 13kT$ )
ZIF-zni (Zn–N)	126	38	95 ( $\approx 14kT$ )
ZIF-zni (Zn–Im)	128	39	96 ( $\approx 14kT$ )

activation process leading to rare events of bond breaking.<sup>29</sup> That is, melting occurs not at the limit of stability of the solid phase but at a point where it is still metastable.

Comparing the potential of mean force for the Zn–Im coordinate (where Im is the center of mass of the imidazolate linker) allows us to distinguish better between the behavior of the different frameworks. In fact, as shown in Table 1, the thermodynamic parameters obtained from Zn–N to Zn–Im potential of mean forces are not the same for the three frameworks. For ZIF-4, there is almost no variation with less than 3% difference for the enthalpic and entropic terms. ZIF-zni shows a similar behavior with less than 3% difference for both terms too. Although these two frameworks show that Zn–N bond breaking can almost be identified to Zn–Im bond breaking in terms of temperature dependence, the story for ZIF-8 is pretty different. In fact, the increase in enthalpy is 43% and even 60% for the entropic term. It explains why ZIF-8 seems to melt at a higher temperature than ZIF-4 as the resulting activation free energy with this reaction coordinate is still equivalent  $11.5 k_B T$  at 1200 K and only goes down to  $7 k_B T$  at 1500 K. Moreover, we observe that there is a large difference between the  $\Delta U^\ddagger$  of the Zn–N coordinate and that of the Zn–Im coordinate in ZIF-8. This shows that the difference in behavior between ZIF-8 and the two other frameworks does not find its root in the intrinsic strength of the Zn–N bond itself (as they are chemically equivalent), but in the influence of the environment of the framework.

**Microscopic Mechanism.** As we have seen, melting appears through creation of defects in the coordination structure, where the Zn–N coordination bonds are broken and later reformed. In our molecular dynamics simulations, we can track directly the formation of such defects by computing the Zn coordination number as a function of framework and temperature. These averaged coordination numbers are shown in an Arrhenius plot on Figure 3. This leads to energies  $\epsilon$  associated with defect formation, which are  $71\text{ kJ mol}^{-1}$  for ZIF-8,  $56\text{ kJ mol}^{-1}$  for ZIF-4, and  $67\text{ kJ mol}^{-1}$  for ZIF-zni. These values are in the same range of magnitude, but we note here again that ZIF-4 exhibits the smallest defect formation energy, in line with thermodynamic and structural properties.

Figure 3 shows the proportion of  $n$ -fold zinc atoms ( $n = 0$  to 5) for the three ZIFs studied, as functions of temperature. For all structures, we see that increase in temperature leads to undercoordination of the zinc atoms through breaking of the Zn–N bonds. The trend we see on the 4-fold coordination matches the structural quantities studied before, as the undercoordination comes at lower temperatures for ZIF-4 (35% drop between 1200 K and 1500 K) but is then much larger for ZIF-8 (66% drop between 1500 K and 1750 K), consistently with a

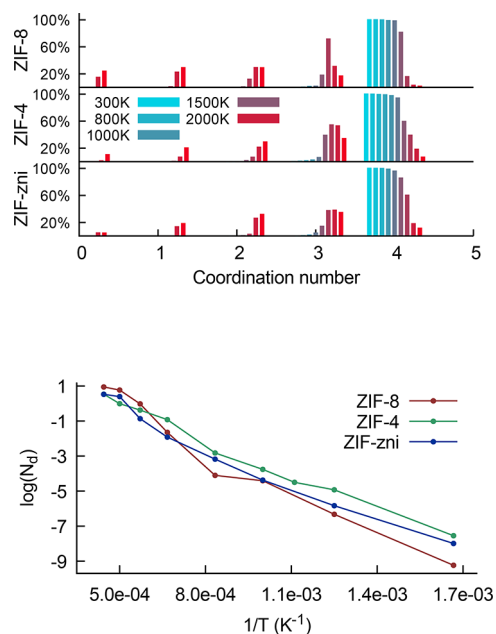


**Figure 3.** Top panel: Distribution of discrete zinc–nitrogen coordination numbers as a function of temperature for ZIF-8, ZIF-4, and ZIF-zni. Bottom panel: van 't Hoff plot of the number of defects. The formation of defects follows an Arrhenius law with respective activation energies of 59, 52, and  $50\text{ kJ mol}^{-1}$  for ZIF-8, ZIF-4, and ZIF-zni.

greater disorganization due to diffusion. ZIF-zni 4-fold coordination really jumps at higher temperatures, with a 45% drop between 1750 K and 2000 K. The microscopic mechanism, which we first unveiled in ZIF-4, is broadly similar in ZIF-8 and ZIF-zni. The transition into the liquid state involves rapid, activated events of imidazolate linker switching from a zinc cation. From an initial 4-fold coordinated zinc, one imidazolate linker moves away and is then replaced by a neighboring Im group with a dangling nitrogen lone pair.

We analyzed these “linker exchange” events, which are depicted in Figure 4. Inspired by Laage et al.’s statistical treatment of the molecular mechanism of reorientation in liquid water,<sup>30,31</sup> we averaged over all events during a molecular dynamics trajectory to plot the average distance of the outgoing and incoming N atoms during an exchange—taking the reference time  $t = 0$  when both nitrogen atoms are at equal distance from the zinc ion. The resulting average dynamic, shown on Figure 4, show that the bond cleavage mechanism is similar for the three frameworks. The only small difference is the coordination state during the exchange for ZIF-8. Although for ZIF-zni, as for ZIF-4, the exchange happens under slight undercoordination ( $\approx -2\%$ ), in the case of ZIF-8 it actually happens under a small overcoordination ( $\approx 3\%$ ). However, this can be explained by the fact that the average coordination number in ZIF-8 liquid is indeed much lower ( $\approx 2.3$ ) than it is in ZIF-4 and ZIF-zni ( $\approx 3.3$ ).

Presented in Table 2 are the activation energies associated with the Zn–N and Zn–imidazolate cleavage frequencies. ZIF-zni shows the highest value ( $137\text{ kJ mol}^{-1}$ ) in terms of activation energy for Zn–N bond breaking which confirms the difficulty to thermodynamically initiate the melting in this framework. In ZIF-4 the two processes were clearly related as the difference in activation energy was only 6.5% more for Zn–Im than for Zn–N. However, for ZIF-8 this difference rises to

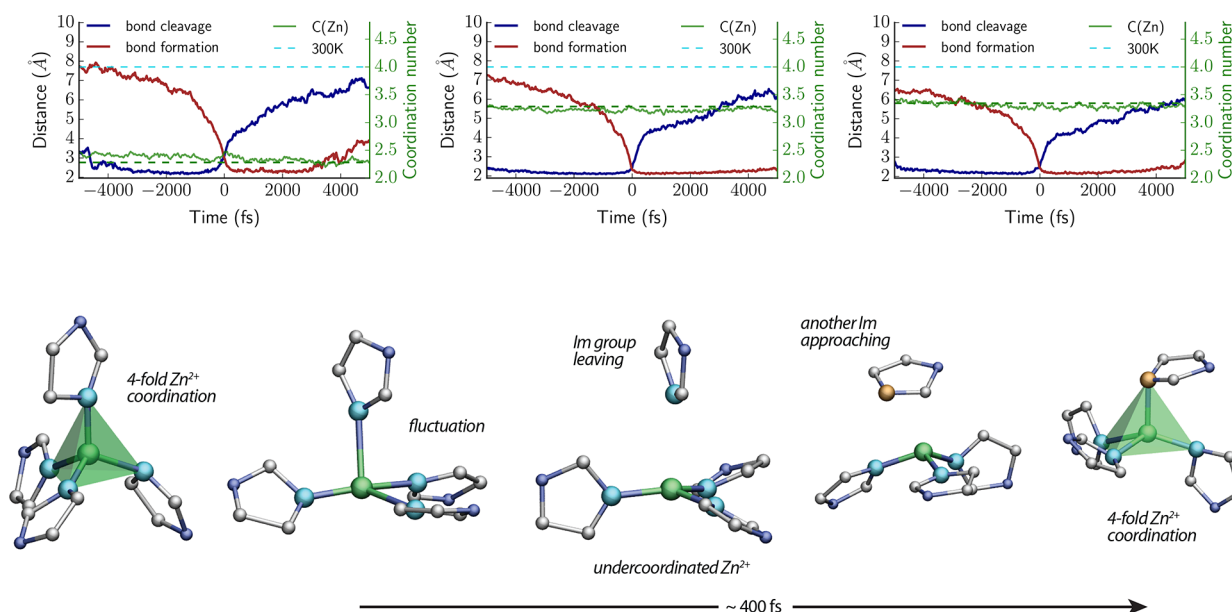


**Figure 4.** Top panel: Behavior during an exchange of a nitrogen atom by another nitrogen atom, in the first coordination sphere of a zinc cation, averaged over all such events (all exchanges on all zinc cations) in the three ZIFs. The distance between the incoming nitrogen and the zinc is plotted in red, and that between the outgoing nitrogen and the zinc in blue. The green curve corresponds to the average coordination number of the zinc cation involved in the exchange. The flat dashed lines are the average coordination number over the whole simulation at 300 (light blue) and 2000 K (green). Bottom panel: Visualization of a representative imidazolate exchange event. Key: Zn, green; N (initially coordinated), light blue; N (coordinated after exchange), orange; C, gray. Bottom panel: Reproduced with permission from ref 15. Copyright 2017 François-Xavier Coudert.

**Table 2. Activation Energies Needed To Break a Zn–N Bonds and Zn–Im/mIm Bonds in the Three ZIFs**

system	$E_a^{\text{Zn-N}}$ (kJ mol <sup>-1</sup> )	$E_a^{\text{Zn-Im/mIm}}$ (kJ mol <sup>-1</sup> )
ZIF-8	112	177
ZIF-4	76	81
ZIF-zni	137	160

58%. This can be understood by looking at the last column in Tables S1–S3. Indeed the proportion of Zn–N cleavage corresponding to a Zn–Im/mIm cleavage is slowly growing in ZIF-4 while it goes from 18% to 94% between 1500 and 2000 K in ZIF-8. ZIF-zni does show a 28% increase between the two activation energies, which can be ascribed to the imidazolate diffusion being hindered due to its denser structure.

**Characterization of the Liquid ZIF.** We have characterized the liquids obtained at temperatures above the melting point by computing, from our FPMD simulations, the translational diffusion coefficients of zinc cations and imidazolate groups (see Table S4). The behavior observed is qualitatively similar to what we saw with the global RMSD presented in Figure S2: diffusion in ZIF-8 starts to be significant at higher temperature than in ZIF-4. For instance at 1500 K,  $D_{\text{Im}}^{\text{ZIF-4}}$  is equal to  $7.7 \times 10^{-10}$  (m<sup>2</sup> s<sup>-1</sup>) which is more than ten times the diffusion coefficient of methylimidazolate in ZIF-8 ( $4.7 \times 10^{-11}$ ) at the same temperature, but this ratio is inverted at 2000 K where  $D_{\text{Im}}^{\text{ZIF-4}}$  is about one-third of  $D_{\text{mIm}}^{\text{ZIF-8}}$ . ZIF-zni shows smaller diffusion coefficients all the way as expected. Nonetheless, the three ZIFs exhibit the same symmetry between the transport of zinc and imidazolate groups, as their diffusion coefficients are always very close, a behavior commonly encountered in classical ionic liquids with strong association.

From the diffusion coefficients at various temperatures, we fitted Arrhenius laws—although we note that there are clearly uncertainties and fluctuations in the values of diffusion coefficients, due to the relatively short trajectories allowed on these large systems by first-principles methods. Characteristic activation energies for all frameworks are presented in Table S4. For example, in the case of Zn, we have the following values: 302 kJ mol<sup>-1</sup> for ZIF-8, 105 kJ mol<sup>-1</sup> for ZIF-4, and 284 kJ mol<sup>-1</sup> for ZIF-zni. The ordering of activation energies associated with diffusion match the one associated with breaking the Zn–imidazolate, thus confirming a diffusive mechanism. Contrary to fully dissociated ionic liquid though, zinc atoms and imidazolate ligands stay strongly associated in average as the aforementioned coordination numbers show.

Finally, when talking about MOFs, porosity is one of the most crucial property that comes to mind. We have thus investigated the porosity of our frameworks as a function of temperature. For that matter, we performed statistical analyses using a probe with a 2.4 Å diameter, the kinetic diameter of helium. The results are presented in Figure 5. ZIF-zni is a dense crystalline structure, with almost no porosity, and as expected this changes very little with temperature (Figure S4). The ZIF-4 liquid, as we demonstrated in previous work, retains most of the modest porosity of its parent crystalline phase, with instantaneous “pockets” or voids in the liquid, even at high temperatures. In stark contrast, ZIF-8—well-known for high porosity of its crystal structure—sees its pore space suffer a lot from the melting process. More than half of its porosity is lost, and the distribution of instantaneous porous volume is rather broad. We note that it is, however, still larger than that of the ZIF-4 liquid.

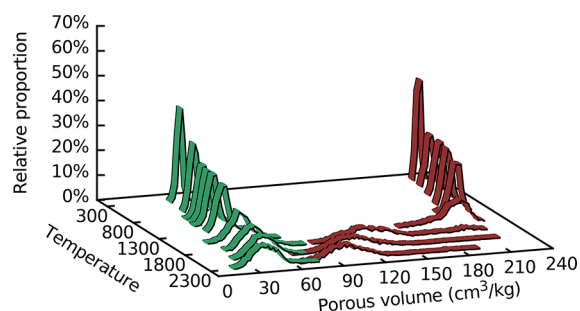


**Figure 5.** Comparison of temperature-dependent porosity between ZIF-4 (green) and ZIF-8 (red). The relative stability of the porous volume in ZIF-4 is striking compared to the collapse of the one in ZIF-8.

## CONCLUSIONS AND PERSPECTIVES

We recently introduced the general term of “MOF liquid”,<sup>15</sup> following a combined experimental and computational study of the melting of ZIF-4, using *in situ* variable temperature X-ray, *ex situ* neutron pair distribution function experiments, and first-principles molecular dynamics simulations. This initial study paved the way for investigations into the questions it had opened, about the generality of the phenomenon and the properties of the MOF liquids. Here, we have used first-principles molecular simulations in order to investigate the question of transferability of the melting phenomenon among three different ZIF frameworks, and the influence of the nature of the parent crystalline ZIF on the physicochemical properties of the resulting liquid. We conclude that the phenomenon is general, and also that the mechanism by which melting occurs is similar in all three frameworks. We also show that there is a clear impact of the characteristics of the ZIF crystals on both the melting, with ZIF-8 melting above its experimental temperature of decomposition, and thus not a candidate. We link this to the high free energy barrier for the detachment of imidazolate linkers from the metal cations. We hypothesize that this may be due to the high porosity of ZIF-8: while for denser ZIFs, like ZIF-4 and ZIF-zni, the movement of the ligand allows it to keep good contact with other ligands and be stabilized by dispersive interactions, in highly porous ZIF-8 the detachment of the imidazolate group implies that it be very isolated in the intermediate state, and thus a high energetic barrier.

Thus, framework topology plays an important role in the determination of melting, as well as in the properties and retention of the porosity in the liquid phase. There is thus a need to study the melting of other ZIF materials, combining experimental and theoretical forces, in order to confirm this hypothesis and establish general criteria for low melting temperatures in ZIFs. This will require the study of ZIFs with different organic ligands, different topologies, but also different metal cations (such as cadmium)<sup>32</sup> that can influence the strength of the zinc–imidazolate interaction—something that has not been studied much to date. The goal would be to provide porous MOF liquids with tunable chemical and physical properties, as is done for crystalline MOF architectures that can be designed and tailored for specific applications. Such materials would be of interest for liquid phase separations, homogeneous catalysis, and ion transport. They could also be used as intermediaries to obtain mechanically and thermally stable porous MOF glasses.

## ASSOCIATED CONTENT

### Supporting Information

The Supporting Information is available free of charge on the ACS Publications website at DOI: 10.1021/acs.jpcc.8b00385.

Total radial distribution function, mean square displacements, activation free energies, porous volumes, crystalline structures, and additional statistics on the mechanism of bond cleavage and diffusion coefficients (PDF)

## AUTHOR INFORMATION

### Corresponding Author

\*(F.-X.C.) E-mail: fx.coudert@chimie-paristech.fr.

### ORCID

François-Xavier Coudert: 0000-0001-5318-3910

### Notes

The authors declare no competing financial interest.

## ACKNOWLEDGMENTS

We thank Anne Boutin, Alain Fuchs, and Thomas Bennett for fruitful discussions. This work benefitted from the financial support of ANRT (thèse CIFRE 2015/0268) and access to HPC platforms provided by a GENCI grant (A0030807069).

## REFERENCES

- Hoskins, B. F.; Robson, R. Infinite polymeric frameworks consisting of three dimensionally linked rod-like segments. *J. Am. Chem. Soc.* **1989**, *111*, 5962–5964.
- Furukawa, H.; Cordova, K. E.; O’Keeffe, M.; Yaghi, O. M. The chemistry and applications of metal-organic frameworks. *Science* **2013**, *341*, 1230444–1230444.
- Bennett, T. D.; Cheetham, A. K.; Fuchs, A. H.; Coudert, F.-X. Interplay between defects, disorder and flexibility in metal-organic frameworks. *Nat. Chem.* **2017**, *9*, 11–16.
- Bennett, T. D.; Cheetham, A. K. Amorphous metal-organic frameworks. *Acc. Chem. Res.* **2014**, *47*, 1555–1562.
- Zhao, Y.; Lee, S.-Y.; Becknell, N.; Yaghi, O. M.; Angell, C. A. Nanoporous transparent MOF glasses with accessible internal surface. *J. Am. Chem. Soc.* **2016**, *138*, 10818–10821.
- Bennett, T. D.; Tan, J.-C.; Yue, Y.; Baxter, E.; Ducati, C.; Terrill, N. J.; Yeung, H. H. M.; Zhou, Z.; Chen, W.; Henke, S.; Cheetham, A. K.; Greaves, G. N. Hybrid glasses from strong and fragile metal-organic framework liquids. *Nat. Commun.* **2015**, *6*, 8079.
- Coudert, F.-X. Responsive metal–organic frameworks and framework materials: under pressure, taking the heat, in the spotlight, with friends. *Chem. Mater.* **2015**, *27*, 1905–1916.
- Bennett, T. D.; Saines, P. J.; Keen, D. A.; Tan, J.-C.; Cheetham, A. K. Ball-milling-induced amorphization of zeolitic imidazolate frameworks (ZIFs) for the irreversible trapping of iodine. *Chem. - Eur. J.* **2013**, *19*, 7049–7055.
- Greaves, G. N.; Meneau, F.; Sapelkin, A.; Colyer, L. M.; ap Gwynn, I.; Wade, S.; Sankar, G. The rheology of collapsing zeolites amorphized by temperature and pressure. *Nat. Mater.* **2003**, *2*, 622–629.
- Colligan, M.; Forster, P. M.; Cheetham, A. K.; Lee, Y.; Vogt, T.; Hriljac, J. A. Synchrotron X-ray powder diffraction and computational investigation of purely siliceous zeolite Y under pressure. *J. Am. Chem. Soc.* **2004**, *126*, 12015–12022.
- Haines, J.; Levelut, C.; Isambert, A.; Hébert, P.; Kohara, S.; Keen, D. A.; Hammouda, T.; Andrault, D. Topologically ordered amorphous silica obtained from the collapsed siliceous zeolite, silicalite-1-F: a step toward “perfect” glasses. *J. Am. Chem. Soc.* **2009**, *131*, 12333–12338.
- Bennett, T. D.; Goodwin, A. L.; Dove, M. T.; Keen, D. A.; Tucker, M. G.; Barney, E. R.; Soper, A. K.; Bithell, E. G.; Tan, J.-C.;

Cheetham, A. K. Structure and properties of an amorphous metal-organic framework. *Phys. Rev. Lett.* **2010**, *104*, 115503.

(13) Bennett, T. D.; Keen, D. A.; Tan, J.-C.; Barney, E. R.; Goodwin, A. L.; Cheetham, A. K. Thermal amorphization of zeolitic imidazolate frameworks. *Angew. Chem., Int. Ed.* **2011**, *50*, 3067–3071.

(14) Bennett, T. D.; Yue, Y.; Li, P.; Qiao, A.; Tao, H.; Greaves, N. G.; Richards, T.; Lampronti, G. I.; Redfern, S. A.; Blanc, F.; Farha, O. K.; Hupp, J. T.; Cheetham, A. K.; Keen, D. A. Melt-quenched glasses of metal-organic frameworks. *J. Am. Chem. Soc.* **2016**, *138*, 3484–3492.

(15) Gaillac, R.; Pullumbi, P.; Beyer, K. A.; Chapman, K. W.; Keen, D. A.; Bennett, T. D.; Coudert, F.-X. Liquid metal-organic frameworks. *Nat. Mater.* **2017**, *16*, 1149–1154.

(16) Coudert, F.-X. Molecular mechanism of swing effect in zeolitic imidazolate framework ZIF-8: continuous deformation upon adsorption. *ChemPhysChem* **2017**, *18*, 2732–2738.

(17) Tan, J. C.; Bennett, T. D.; Cheetham, A. K. Chemical structure, network topology, and porosity effects on the mechanical properties of zeolitic imidazolate frameworks. *Proc. Natl. Acad. Sci. U. S. A.* **2010**, *107*, 9938–9943.

(18) VandeVondele, J.; Krack, M.; Mohamed, F.; Parrinello, M.; Chassaing, T.; Hutter, J. Quickstep: fast and accurate density functional calculations using a mixed Gaussian and plane waves approach. *Comput. Phys. Commun.* **2005**, *167*, 103–128.

(19) <http://www.cp2k.org>, accessed 8 March 2018.

(20) VandeVondele, J.; Krack, M.; Mohamed, F.; Parrinello, M.; Chassaing, T.; Hutter, J. Quickstep: Fast and accurate density functional calculations using a mixed Gaussian and plane waves approach. *Comput. Phys. Commun.* **2005**, *167*, 103–128.

(21) Bussi, G.; Donadio, D.; Parrinello, M. Canonical sampling through velocity rescaling. *J. Chem. Phys.* **2007**, *126*, 014101.

(22) Perdew, J. P.; Burke, K.; Ernzerhof, M. Generalized gradient approximation made simple. *Phys. Rev. Lett.* **1996**, *77*, 3865–3868.

(23) Grimme, S.; Antony, J.; Ehrlich, S.; Krieg, H. A consistent and accurate ab initio parametrization of density functional dispersion correction (DFT-D) for the 94 elements H-Pu. *J. Chem. Phys.* **2010**, *132*, 154104.

(24) Haigis, V.; Coudert, F.-X.; Vuilleumier, R.; Boutin, A. Investigation of structure and dynamics of the hydrated metal-organic framework MIL-53(Cr) using first-principles molecular dynamics. *Phys. Chem. Chem. Phys.* **2013**, *15*, 19049–19056.

(25) Goedecker, S.; Teter, M.; Hutter, J. Separable dual-space Gaussian pseudopotentials. *Phys. Rev. B: Condens. Matter Mater. Phys.* **1996**, *54*, 1703–1710.

(26) Pinheiro, M.; Martin, R. L.; Rycroft, C. H.; Jones, A.; Iglesia, E.; Haranczyk, M. Characterization and comparison of pore landscapes in crystalline porous materials. *J. Mol. Graphics Modell.* **2013**, *44*, 208–219.

(27) Martin, R. L.; Smit, B.; Haranczyk, M. Addressing challenges of identifying geometrically diverse sets of crystalline porous materials. *J. Chem. Inf. Model.* **2012**, *52*, 308–318.

(28) Willems, T. F.; Rycroft, C. H.; Kazi, M.; Meza, J. C.; Haranczyk, M. Algorithms and tools for high-throughput geometry-based analysis of crystalline porous materials. *Microporous Mesoporous Mater.* **2012**, *149*, 134–141.

(29) Samanta, A.; Tuckerman, M. E.; Yu, T.-Q.; E, W. Microscopic mechanisms of equilibrium melting of a solid. *Science* **2014**, *346*, 729–732.

(30) Laage, D. A molecular jump mechanism of water reorientation. *Science* **2006**, *311*, 832–835.

(31) Laage, D.; Hynes, J. T. On the molecular mechanism of water reorientation. *J. Phys. Chem. B* **2008**, *112*, 14230–14242.

(32) Baxter, E. F.; Bennett, T. D.; Cairns, A. B.; Brownbill, N. J.; Goodwin, A. L.; Keen, D. A.; Chater, P. A.; Blanc, F.; Cheetham, A. K. A comparison of the amorphization of zeolitic imidazolate frameworks (ZIFs) and aluminosilicate zeolites by ball-milling. *Dalton Trans.* **2016**, *45*, 4258–4268.